Arch Virol
DOI 10.1007/s00705-016-3013-6

ORIGINAL ARTICLE

Exploration of the BF2*15 major histocompatibility complex class I binding motif and identification of cytotoxic T lymphocyte epitopes from the H5N1 influenza virus nucleoprotein in chickens

Weijun Zhang[2] · Qinghua Huang[1] · Mei Lu[3] · Fengzhu Zhu[4] · Yan-yan Huang[1] · Shao-hua Yang[1] · Zhengjie Kong[4] · Xiu-mei Zhang[1] · Chuan-tian Xu[1]

Received: 29 March 2016 / Accepted: 6 August 2016
© Springer-Verlag Wien 2016

Abstract The binding motif of BF2*15 major histocompatibility complex (MHC) class I was explored by analyzing the interaction between an infectious bronchitis virus octapeptide and BF2*15, and the cytotoxic T lymphocyte (CTL) epitope from the nucleoprotein (NP) of H5N1 virus was identified using experimental methods. Computational methods, including homology modeling, molecular dynamics simulation, and molecular docking analysis, were used. The recombinant plasmid pCAGGS-NP was constructed, and NP expression was confirmed by indirect immunofluorescence and Western blot in transfected 293T cells. Antibodies against NP in pCAGGS-NP-inoculated specific-pathogen-free chickens were detected by enzyme-linked immunosorbent assay (ELISA). Interferon γ (IFN-γ) mRNA was quantified, and IFN-γ production was evaluated using quantitative reverse transcription PCR and capture ELISA, respectively. $CD8^+$ T-lymphocyte proliferation was detected using flow cytometric analysis. The BF2*15 MHC class I binding motif "x-Arg/Lys-x-x-x-Arg/Lys" was explored. Quantification of chicken IFN-γ mRNA, evaluation of IFN-γ production, and measurement of $CD8^+$ T-lymphocyte proliferation confirmed that the peptide $NP_{67–74}$ of H5N1 was the BF2*15 MHC-class-I-restricted CTL epitope.

W. Zhang and Q. Huang contributed equally to this work.

✉ Chuan-tian Xu
xcttaian2002@163.com

[1] Shandong Key Lab of Animal Disease Control and Breeding, Institute of Animal Science and Veterinary Medicine, Shandong Academy of Agricultural Sciences, Jinan 250100, Shandong, People's Republic of China

[2] School of Social Development and Public Policy, China Institute of Health, Beijing Normal University, 19 Xinjiekou Wai St., Beijing 100875, People's Republic of China

[3] Weifang Engineering Vocational College, Qingzhou 262500, Shandong, People's Republic of China

[4] College of Animal Science, Shandong Agricultural University, Tai'an 271018, Shandong, People's Republic of China

Introduction

Influenza A viruses infect a wide variety of animal species, including birds, humans, pigs, and other mammals [1]. The unabated circulation of highly pathogenic H5N1 avian influenza viruses has been a serious threat to public health worldwide [2]. Cross-species infection is considered the fundamental mechanism of initiation of human influenza pandemics [3]. In 1997, a highly pathogenic H5N1 avian influenza virus (HPAI) was transmitted directly from poultry to humans with an overall case-fatality rate of 33 % in Hong Kong [4, 5]. Similarly, HPAI H5N1, which is especially deadly for poultry, has been causing poultry outbreaks in Asia almost continuously since 2003. This virus is now endemic in several countries and continues to be the animal influenza virus of greatest concern for human health. Furthermore, from the end of 2003 to January 2015, 777 laboratory-confirmed human cases of H5N1 virus infection from 16 countries have been reported to the World Health Organization. Of these cases, 428 (55.1 %) were fatal because of acute respiratory distress syndrome, multiple organ dysfunction, lymphopenia, and hemophagocytosis [4–6]. In view of the high frequency of naturally occurring mutations, the lethality of H5N1 raises considerable concern about the potential transmissibility of the virus in humans [2].

Published online: 12 August 2016

Developing a potent vaccine for influenza A virus that provides long-lasting immunity is a difficult task [7]. This challenge may be due to the antigenic drift of the virus, in which the circulating strain in an infectious cycle differs from the previously circulating strain [8–10]. To efficiently prevent a future influenza pandemic, a robust global surveillance system should be strengthened for the timely detection of novel H5N1 virus strains in animals once they arise [11]. On the other hand, effective vaccines, including inactivated viral vaccines and live-attenuated, cold-adapted H5N1 vaccines, could also be developed for the prevention of H5N1 virus infection through large-scale vaccination [12–14]. In addition, other forms of H5N1 vaccines, including those based on DNA, proteins, viral vectors, and virus-like particles as well as a number of combination vaccinations, are in the developmental stage or in preclinical or clinical trials, some of which have shown efficacy in preventing H5N1 infections [2, 15–21]. Theoretically, the rational development of future vaccines will require a systematic understanding of the protective humoral and cellular immune responses that occur during H5N1 virus infection. Furthermore, this pursuit should aim to induce a broad immune response that accommodates the plasticity of major antigenic sites. Recent research has indicated that cell-mediated immunity may play a very important role in the clearance of influenza virus [8]. Therefore, a vaccine generating robust T-cell immunity against influenza should be paid more attention. Major histocompatibility complex (MHC) I-restricted cytotoxic T lymphocytes (CTLs) can kill virus-infected cells and eliminate potential sources of new virus [22–24]. Furthermore, T-cell recognition of the peptide–MHC complex is a prerequisite for cellular immunity. Hence, identifying CTL epitopes is crucial in the design of synthetic vaccines and understanding the immune mechanisms involved in the clearance of viral infection [25]. A number of studies successfully identified pathogen-derived T-cell epitopes from H5N1 virus in humans [7, 26–30] and mice [31, 32]. A range of computational algorithms have been developed to predict CTL epitopes in pathogen protein sequences. These algorithms are based on specific MHC class I anchor motifs [33–35], a weight-matrix method for identifying amino acids that occur at a higher-than-expected frequency at specific epitope positions [36–38], or artificial neural networks (ANNAs) [36, 39, 40]. The accuracy of these methods has also been demonstrated by their prediction of the vast majority of CTL epitopes [41].

Unlike many other hosts, knowledge is limited on the specific H5N1-derived peptides targeted by T cells in chickens. To date, two studies have reported on T-cell epitopes in the nucleoprotein (NP) and hemagglutinin (HA) of H5N1 virus in chickens [42, 43]. In these proteins, $NP_{89–97}$ and $NP_{198–206}$ were identified as T-cell epitopes in chickens of certain haplotypes [43], and $H5_{246–260}$ within HA1 domain was identified as a dual-specific epitope, which was found to be presented by both major MHC class I and II molecules in chickens of the B^{19} haplotype [42]. In 2007, Liu et al. reported a chicken MHC-I (BF2*15)/peptide tetramer [44], indicating that an octapeptide (WRRQARYK) from the infectious bronchitis virus (IBV) 52 strain [45] is able to bind to the B15 haplotype and induce an immune response.

This study has two objectives. Our first objective is to explore the interaction between the IBV octapeptide and BF2*15 and to further identify the binding motif of BF2*15 using computational methods, such as homology modeling, molecular dynamics (MD) simulation, and molecular docking. The second objective is to experimentally identify the CTL epitopes from the NP of A/Goose/Gongdong/1/96 (H5N1) virus of MHC class I (BF2*15) based on the above motif in chickens.

Materials and methods

Sequence of BF2*15 and Chβ-2M

Coding region sequences of BF2*15 and the Chβ-2M gene were obtained from GenBank (accession numbers L28958 and M84767). The protein sequence features were based on information from UniProtKB (accession numbers Q9GIP6 and P21611).

Structure prediction of BF2*15 MHC class I

First, a BLAST search was conducted to search template structures of chicken MHC haplotypes in the PDB (Protein Data Bank) database. Second, sequence alignment was performed between target and template sequences, and the template structure with higher sequence similarity and sequence identity were selected for homology modeling using the Modeler 9v6 software package. Third, to fully refine the constructed structure by homology modeling, molecular dynamics simulation was performed by using the Nanoscale Molecular Dynamics (NAMD) 2.7 software package under the CHARMM (Chemistry at Harvard Molecular Mechanics) force field [46]. The software is parallel molecular dynamics code designed for the high-performance simulation of large biomolecular systems by the University of Illinois [47]. Prior to such refinement, the protein–peptide complex was solvated in a cubic water box. The periodic condition was used, and the cutoff was set to 10 Å. Fourth, protein docking was performed using the ZDOCK software package [48]; the software can evaluate possible interaction relationships between two proteins by its rigid docking and scoring function. Fifth, the

RDOCK program of the ZDOCK software package was used to refine the interaction relationship between BF2*15 and the IBV octapeptide, and the additional RDOCK score was adopted to further determine the proper interaction relationship between the two molecules.

Structural feature analysis of the IBV octapeptide

The CTL peptide "WRRQARYK" is the amino acid sequence 71–78 of the NP from IBV. The IBV octapeptide was constructed directly by the Build and Edit Protein module in Discovery Studio Visualizer. The initial conformation of the IBV octapeptide is linear, and MD simulation was performed to explore the conformational space of the octapeptide. Four trajectories were simulated, with 50 ns for each trajectory.

Analysis of the interaction between BF2*15 and the IBV octapeptide

We performed protein docking between BF2*15 and the IBV octapeptide. Two thousand different conformations were obtained and then grouped into 100 clusters. A total of 23 conformations with ZDOCK scores higher than 14 from diverse clusters were selected. Afterward, RDOCK was performed against these 23 conformations, and eight conformations were finally selected as promising conformations for interaction relationship analysis. Concurrently, MD simulation was performed for all of the eight conformations. Specifically, when the octapeptide dissociated from BF2*15, the simulation was stopped, and the corresponding conformation was considered the default conformation. Eventually, the anchor residues and the binding motif of BF2*15 were determined on the basis of the analysis.

Prediction and synthesis of the peptide from the H5N1 virus NP

Initially, sequence analysis showed eight octapeptides from the NP of the H5N1 influenza virus (Table 2), particularly "GKDPKKTG," "RRRDGKWV," "DKEEIRRI," "IRRIWRQA," "TRALVRTG," "IRMIKRGI," "DRNF WRGE," and "TRVAPRGQ." Considering that the BF2*15 groove is extremely negatively charged, the octapeptides with an excessive number of negatively charged residues, such as "DKEEIRRI" and "DRNFWRGE," were excluded. Concurrently, the docking results above also indicated that the Arg at P3 position considerably facilitated octapeptide binding. Hence, the peptide "GKDPKKTG" was further excluded for its Asp3 with a negative charge. Then, the remaining five peptides were subjected to MD simulation to explore their conformations in solvent. Specifically, each peptide was simulated with four trajectories for 50 ns, and the structure with the lowest potential energy was selected and used for molecular docking. We identified P2 and P6 residues as anchor residues; thus, only the conformations with the highest ZDOCK score, as well as those with anchor residues interacting with Asp24, Asp73, and Asp113, were selected. MD simulations were performed against these complexes using the previously described procedure to obtain their interaction relationship. For each octapeptide and BF2*15 complex, three trajectories were simulated for at least 50 ns. By using the MD simulation, we found that the TRVAPRGQ octapeptide dissociated from the BF2*15 groove rapidly, and therefore the octapeptide "TRVAPRGQ" was also excluded.

All peptides, including $NP_{120–128}$ (TRALVRTGM), $NP_{163–170}$ (IRMIKRGI), $NP_{85–92}$ (IRRIWRQA), $N_{P67–74}$ (RRRDGKWV), and the irrelevant peptides $NP_{71–78}$ (WRRQARYK) from the NP of the IBV, were synthesized by Scilight Biotechnology LLC (Beijing, China). These peptides were purified to >95 % using high-performance liquid chromatography.

Chickens

All of the BF2*15 white Leghorn specific-pathogen-free (SPF) chickens used in this study were obtained from the Experimental Animal Center of Poultry, Institute of Shandong Academy of Agricultural Science.

Viruses and cell lines

The isolate A/Goose/Gongdong/1/96 (H5N1) and the 293T cells were part of our laboratory collection.

NP expression plasmid pCAGGS-NP

The plasmid pCAGGS-NP was constructed and cloned into the plasmid vector pCAGGS under the control of the chicken β-actin promoter. The NP gene was obtained from the isolate A/Goose/Gongdong/1/96 (H5N1) by PCR (the oligonucleotide sequences are available upon request). The plasmid was named pCAGG-NP. The expression of the NP protein from the plasmid was confirmed by indirect immunofluorescence assay and Western blot of plasmid-transfected 293 T cells.

Immunization of SPF chickens with plasmid pCAGGS-NP

For DNA vaccine immunizations, 15 three-week-old SPF chickens were separated into two groups in which 10 were immunized twice with 100 mg of pCAGGS-NP in their leg

muscle at three-week intervals. By contrast, five chickens were injected with the same volume of PBS as controls. Sera were collected weekly for NP antibody detection.

Detection of NP antibody

Serum antibodies to AIV NP were detected using an indirect ELISA method described previously, which uses prokaryotically expressed NP as antigen [49]. The testing steps were as follows. After washing the plates, 50 mL of the test serum was mixed in the test wells with 50 mL of antigen diluted to 1:10 in ELISA buffer. After incubation at 37 °C for 1 h, 100 mL of horseradish peroxidase conjugate (diluted to 1:1000 in ELISA buffer) was added to each well. The plates were then further incubated at 37 °C for 1 h. After two washing steps, 100 mL of TMB substrate was added and incubated at room temperature for 10 min. The reaction was stopped by adding 100 mL of 2 M H_2SO_4. The extinctions were measured at 490 nm with a micro ELISA reader (Bio-Rad).

Preparation of splenic lymphocytes

To prepare splenic lymphocytes, all 10 pCAGGS-NP immunized chickens were sacrificed by cardiac puncture blood collection on day 28 after the first immunization. Sterile spleens were collected and filtered through a sieve screen using a syringe plunger to obtain a single-cell suspension in tissue culture medium (RPMI 1640, Gibco BRL NY, USA). Cell suspensions were overlaid onto a Histopaque 1077 density gradient medium and centrifuged at 1800 rpm for 20 min at 18 °C. The lymphocytes were collected from the interface, washed three times in RPMI, and counted using a Trypan blue dye exclusion assay.

$CD8^+$ T lymphocyte proliferation assay

The splenic lymphocytes collected from the 10 immunized chickens were stained with 5 mM CFSE (Invitrogen) prewarmed in PBS for 10 min, washed three times, and suspended in RPMI 1640 containing 2 mM L-glutamine, 100 IU mL^{-1} penicillin, 100 IU mL^{-1} streptomycin, and 10 % fetal bovine serum (R10 medium). The cells were plated at 10^6 $well^{-1}$ in 24-well plates with RPMI 1640 medium before stimulation for three days with 100 mg mL^{-1} of the four peptides generated from NP and the unrelated peptide $N_{71–78}$ of IBV. Subsequently, the cells were washed with PBS and stained using anti-CD8-PE before flow cytometric analysis. Flow cytometry was performed on a Cytomics FC 500 MCL (Beckman) flow cytometer, and the results were analyzed with its embedded software CXP. Two repeats were performed simultaneously for each peptide during flow cytometry.

Detection of IFN-γ gene expression by fluorescent quantitative PCR

Total RNA from spleen cells cultured for 48 h was extracted using TRIzol Reagent. A one-step reverse-transcription PCR (RT-PCR) kit was used for reverse transcription to obtain the cDNA. On the basis of the IFN-γ standard curve established in this laboratory, we used the cDNA as the template for the fluorescent quantitative PCR detection of the samples. The avian β-actin gene was used as a reference gene. The copy number of IFN-γ mRNA in each gene was calculated using the Ct values of the fluorescence and standard curves. The expression level of IFN-γ mRNA is the ratio of the total copies of the IFN-γ and β-actin genes. The normalized value of each sample was calculated using the following formula: normalized value = concentration of target gene/concentration of reference gene. The multiple in the differential expression of target genes in the tested group was calculated by comparing with target genes in the control group. The mean value and standard deviation ($\bar{X} \pm$ SD) of the normalized values of all samples in the tested and control groups were counted.

Establishment of the ELISA standard curve of IFN-γ

On the basis of the standard procedure for IFN-γ ELISA, we used a Rayto RT-6100 microplate reader for readings at 450 nm. The "Logistic curve fitting 2 (four parameters)" model was used to obtain the ELISA standard curve. The optical density values of the sample and control groups were fitted into the standard curve to determine the IFN-γ concentrations.

Statistical analysis

All statistical analysis was performed using SPSS statistics 17.0 software. The indirect ELISA (iELISA) antibody was statistically compared using Student's *t*-test to assess differences between groups. The percentage of $CD8^+$ T lymphocytes, the normalized values of IFN-γ mRNA, and the optical density values of IFN-γ were analyzed using analysis of variance (ANOVA), and a probability value below 0.05 was considered significant. All data were expressed as mean ± standard deviation (SD).

Results

Structure prediction of BF2*15 MHC

Four chicken MHC haplotype structures, namely, B2 [50], B4 [51], B14 [50], and B21 [52], were resolved. Herein, we used two BF2*21 structures (3BEV and 3BEW) as

templates to construct the BF2*15 structure. The sequence similarity and identity were 95.4 % and 93.2 %, respectively. Furthermore, the resolutions of 3BEV and 3BEW were 2.1 and 2.6 Å, respectively, indicating considerable reliability. The constructed BF2*15 structure was extremely similar to those of other chicken MHCs (Fig. 1). In addition, the root-mean-square deviation between BF2*15 and 3BEV or 3BEW was 0.684 or 0.649 Å, respectively (Fig. 2). Hence, we acquired the structure of BF2*15 with the lowest potential energy conformation (Fig. 3).

Structural feature analysis of the IBV octapeptide WRRQARYK

The IBV octapeptide was directly constructed by the Build and Edit Protein module of Discovery Studio Visualizer. The initial conformation of the IBV octapeptide was linear, and MD simulation was performed to explore the conformational space of the octapeptide. Four trajectories were simulated, with 50 ns for each trajectory. The lowest potential energy conformation was selected for further molecular docking (Fig. 4). As shown by the analysis, the IBV octapeptide was positively charged because of the presence of four positive residues and the absence of any

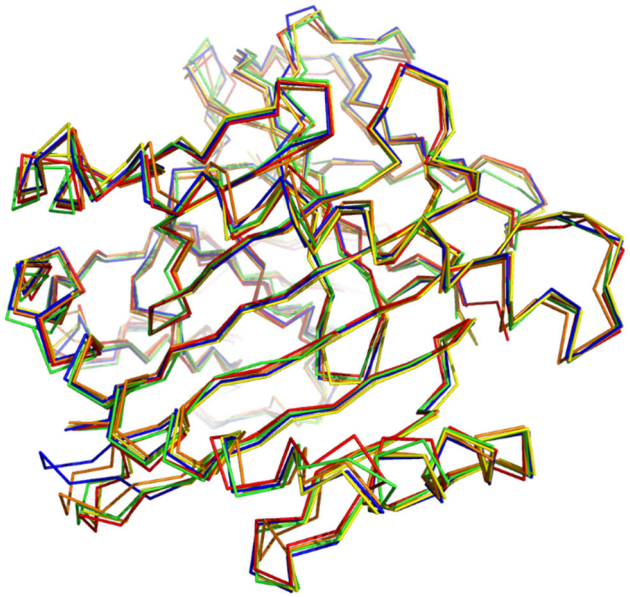

Fig. 1 Comparison of constructed B15, B2 (4CVX), B4 (4E0R), B14 (4CW1) and B21 (3BEV). All of these proteins are shown as ribbons, and are colored green (B15), blue (B2), orange (B4), yellow (B14) and red (B21). Molecular dynamics (MD) simulation was performed for BF2*15 in an explicit solvent model. Three trajectories were used, and each trajectory lasted 30 nanoseconds (ns). After MD simulation, the constructed protein structure was refined to its natural conformation. We observed that the protein structure is stable, with RMSD fluctuation less than 1 angstrom. The conformation with the lowest potential energy was extracted for further simulation (color figure online)

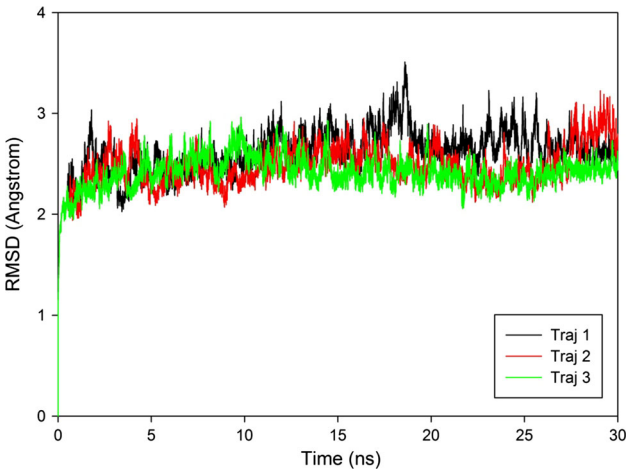

Fig. 2 RMSD analysis of BF2*15 simulation trajectories. Black, trajectory 1; red, trajectory 2; green, trajectory 3 (color figure online)

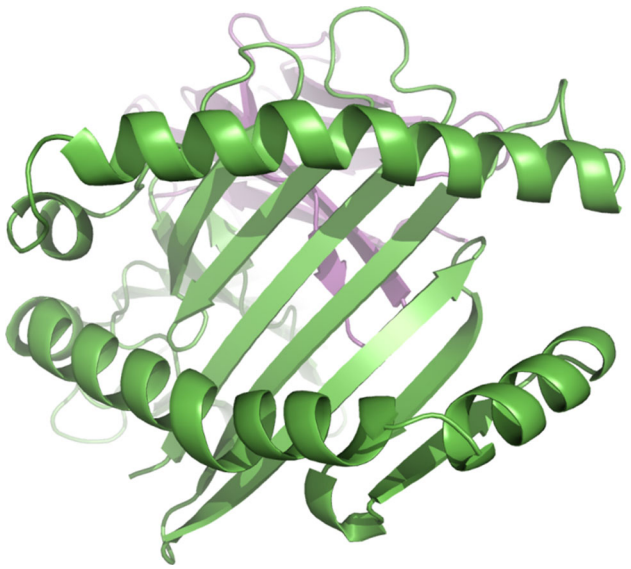

Fig. 3 Top view of the lowest potential energy conformation of BF2*15. Green and purple cartoons represent BF2*15 and β-2M, respectively (color figure online)

negative residues. In addition, the free amino group of Trp1 also contributed to the positive potential. The free carboxyl moiety of Lys8 interacted with the Arg3 side chain, partially neutralizing the positive charge and generating the cyclic conformation of the octapeptide.

Interaction between BF2*15 and the IBV octapeptide

Eight conformations with the highest ZDOCK scores were finally selected as promising conformations for interaction relationship analysis (Fig. 5). Eventually, octapeptides from only one conformation remained associated in the 116-ns simulation. Under this condition, the peptide

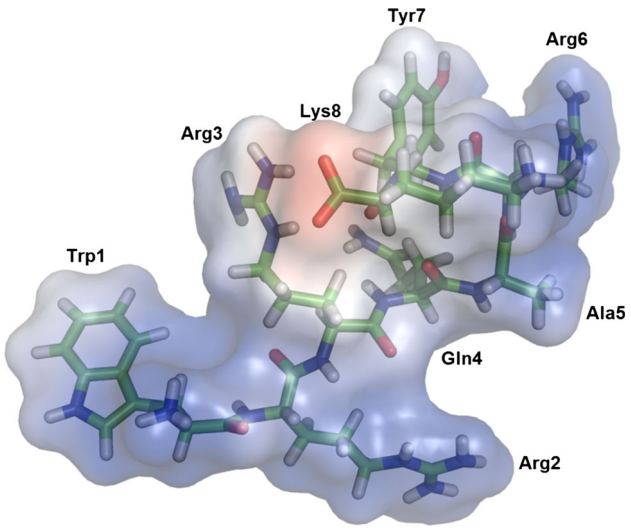

Fig. 4 The lowest potential energy conformation of the IBV octapeptide, shown by colored sticks and electrostatic potential surface. Green, red, blue and white sticks indicate carbon, oxygen, nitrogen and hydrogen atoms, respectively. Blue and red surfaces indicate positively and negatively charged electrostatic potential, respectively (color figure online)

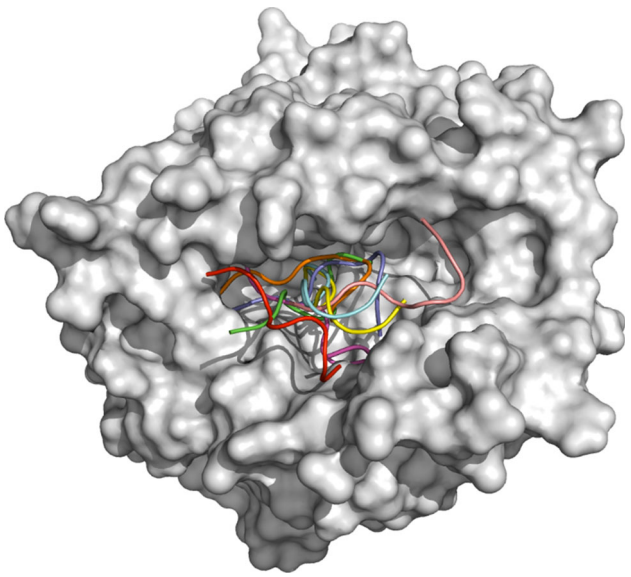

Fig. 5 Possible interactions between BF2*15 and the IBV octapeptide. BF2*15 is displayed as a surface, and the IBV octapeptide is shown as a cartoon in different colors. MD simulation was performed for all eight conformations. When the octapeptide dissociated from BF2*15, the simulation was stopped and the corresponding conformation was considered the default conformation. Ultimately, the octapeptide from only one conformation remained associated in a 116-ns simulation

became extended, and the lowest potential energy conformation showed that the octapeptide fully occupied the BF2*15 binding groove (Fig. 6). Evidently, Arg2 and Arg6 oriented into the binding groove and formed salt bridges with Asp24/Asp73 and Asp73/Asp113, respectively. Moreover, the free amino moiety of Trp1 formed electrostatic interactions with Glu62 of BF2*15, and the main-chain oxygen formed a hydrogen bond with the Tyr7 side chain. A complicated hydrogen-bond network was formed between Arg3, Ala5, and Gln4 of the octapeptide and Tyr149, Tyr97, and Thr64 of BF2*15, respectively. These hydrogen bonds greatly enhanced the interaction stability between the peptide and the MHC.

The findings showed that Arg2 and Arg6 can act as anchor residues and contribute the most to the interaction. Other residues, such as Tyr7, are either incapable of interacting with BF2*15 or interact by main-chain atoms, such as pTrp1, pGln4, and pAla5. In addition, the electrostatic interaction between Lys8 and Asp148 was exposed to the solvent, decreasing the interaction's stability. Hence, in this sense, Arg2 and Arg6 are the most important residues. Given that these two residues were both positively charged, we presume that Lys is also suitable residue. Thus, we speculate that the binding motif was x-Arg/Lys-x-x-x-Arg/Lys-x-x.

The sequence alignment of B15 with B2, B4, B14, and B21 indicate that the peptides differed at residues 24, 73, and 113 (Table 2).

Peptide prediction of the H5N1 virus NP protein

On the basis of MD simulation, we found that the octapeptide "RRRDGKWV" formed a stable interaction with BF2*15 (Fig. 7). Specifically, the octapeptide "RRRDGKWV" partly occupied the BF2*15 groove; however, its interaction mode differed from that of the IBV octapeptide. The Arg1 side chain, instead of main chain, interacted with BF2*15 Glu62 as well as Asp24. However, Arg2 interacted with Asp73/Asp113 and replaced the position of Lys6. Although the interaction relationships were dissimilar, we cannot conclude that the octapeptide "RRRDGKWV" is incapable of binding with BF2*15, because the interaction was stable over the entire simulation process, with multiple salt bridges and hydrogen bonds formed between the peptide and BF2*15. The octapeptide "IRRIWRQA" (Fig. 8) also bound to BF2*15. The octapeptide exhibited a similar binding mode with "RRRDGKWV," and Arg2 of the octapeptide "IRRIWRQA" also interacted with Asp73 and Asp113 instead of Asp24. However, the difference in "IRRIWRQA" was that Arg3 of octapeptide "IRRIWRQA" played the role in interacting with Glu62 and Asp24. The free carboxyl moiety of Ala8 formed electrostatic interactions with Lys83 and Lys143, greatly neutralizing the positive potential outside the binding groove.

The octapeptide "TRALVRTG" bound with BF2*15 in a way that was similar to that of the IBV octapeptide. The peptide fully occupied the groove with a more extended conformation than the other octapeptide. Two anchor

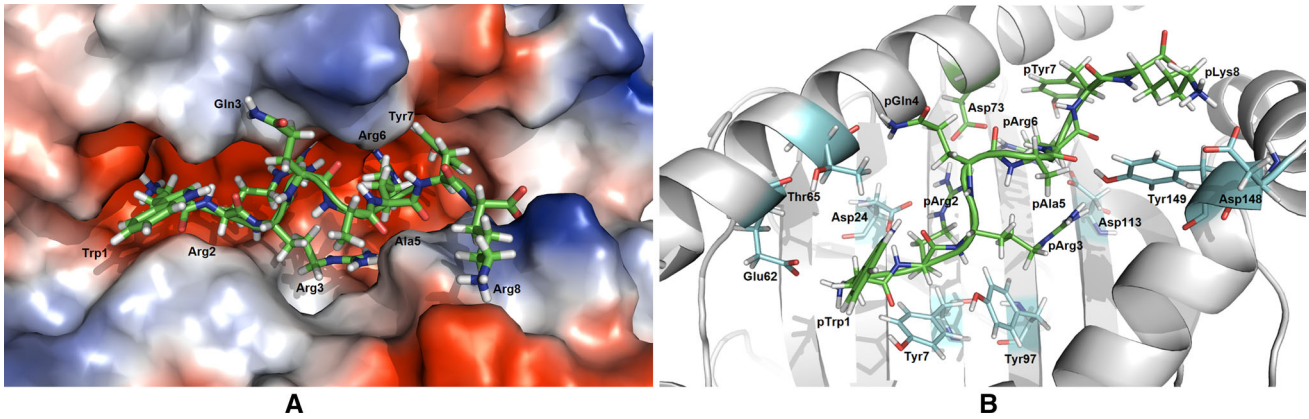

Fig. 6 The lowest potential energy conformation of the BF2*15-IBV octapeptide complex, shown as an electrostatic potential surface (A) and sticks as well as cartoons (B). Based on the interaction model we constructed, we can conclude that Arg2 and Arg6 act as anchor residues and contribute the most to the interaction. Other residues are either incapable of interacting with BF2*15, like Tyr7, or interact by main chain atoms, like pTrp1, pGln4 and pAla5. The electrostatic interaction between Lys8 and Asp148 is exposed to solvent, decreasing its stability. Therefore, Arg2 and Arg6 are the most important residues. Given that these two residues are both positively charged, we presume that Lys is also suitable

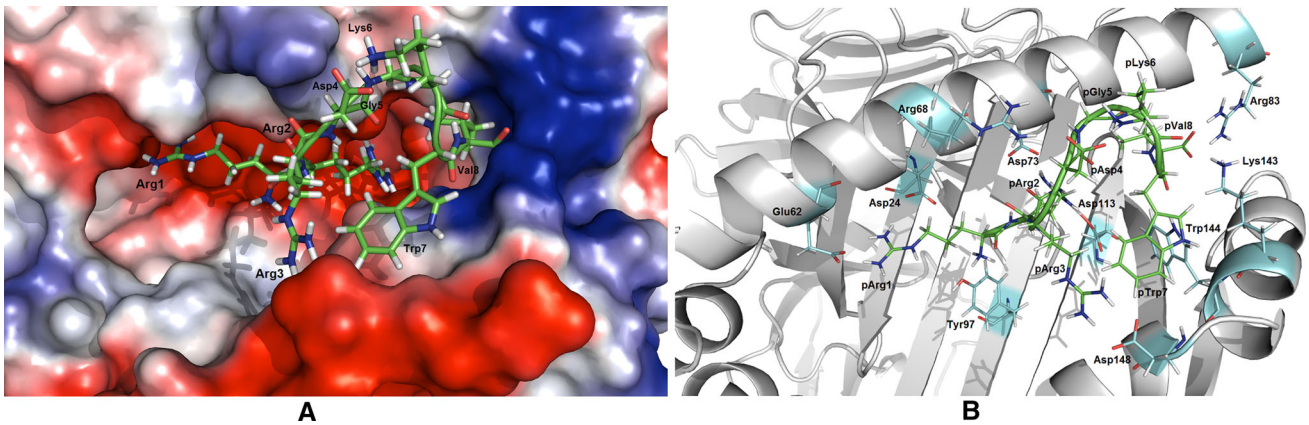

Fig. 7 The lowest potential energy conformation of the BF2*15-RRRDGKWV octapeptide complex, shown as an electrostatic potential surface (A) and sticks as well as cartoons (B). As for the IRRIWRQA octapeptide, it is able to bind with BF2*15. It has a binding mode similar to that of the RRRDGKWV octapeptide, and Arg2 of the IRRIWRQA octapeptide also interacts with Asp73 and Asp113 instead of Asp24. However, the difference is that Arg3 of the IRRIWRQA octapeptide plays the role of interacting with Glu62 and Asp24. The free carboxyl moiety of Ala8 forms an electrostatic interaction with Lys83 and Lys143, greatly neutralizing the positive potential outside the binding groove

residues, Arg2 and Arg6, interacted with Asp24/Asp73 and Asp73/Asp113, respectively. The free amino moiety of Thr1 formed a salt bridge with Glu62 and a hydrogen bond with Tyr156. Arg2 also formed another hydrogen bond with Tyr97. Finally, the free carboxyl moiety of Gly8 formed an electrostatic interaction with Lys143. The octapeptide "IRMIKRGI" also bound with BF2*15 (Fig. 9). However, the binding ability was weak, which was mainly due to the octapeptide's cyclic conformation. The free carboxyl moiety of Ile8 interacted with Arg2 and Arg6, leading to weaker electrostatic interactions of Arg2/Arg6 and Asp24/Asp73/Asp113. Furthermore, the free carboxyl moiety of Ile8 failed to interact with Lys83 or Lys143.

Detection of NP antibody

The expression efficiency of pCAGGS-NP was confirmed by IFA and Western blot (Fig. 10). To assess the immune effects of the vaccine, serum NP antibody was detected using indirect ELISA. Compared with the control group, a significant increase ($P < 0.01$) in blood NP antibody was observed in the immunized group at two weeks after the first vaccination. After the boost, the blood NP antibody level of the immunized group increased further and remained at a high level throughout the duration of the experiment (Fig. 11). This finding indicated that the immune systems of the chickens were activated by vaccine immunization.

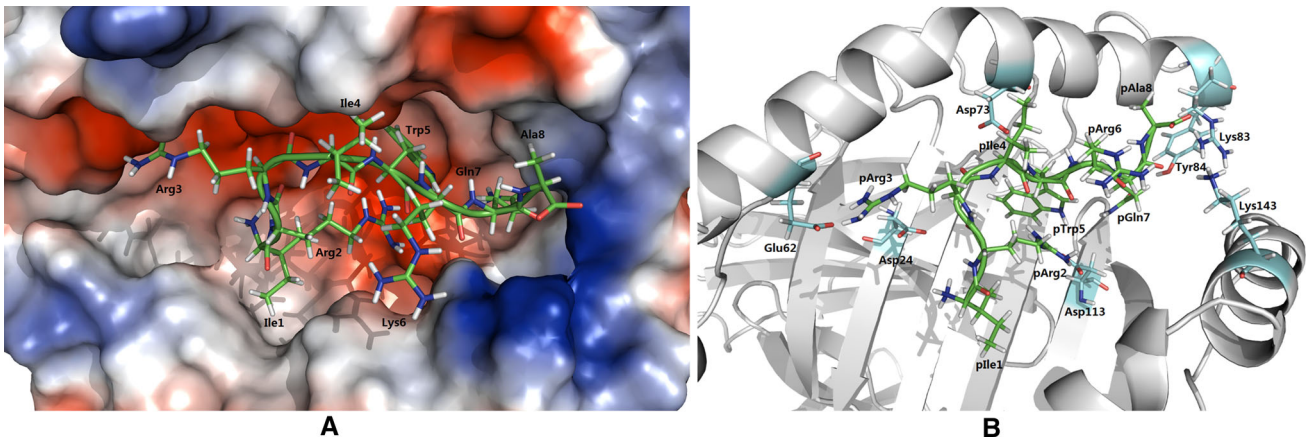

Fig. 8 The lowest potential energy conformation of the BF2*15-IRRIWRQA octapeptide complex, shown as an electrostatic potential surface (A) and sticks as well as cartoons (B)

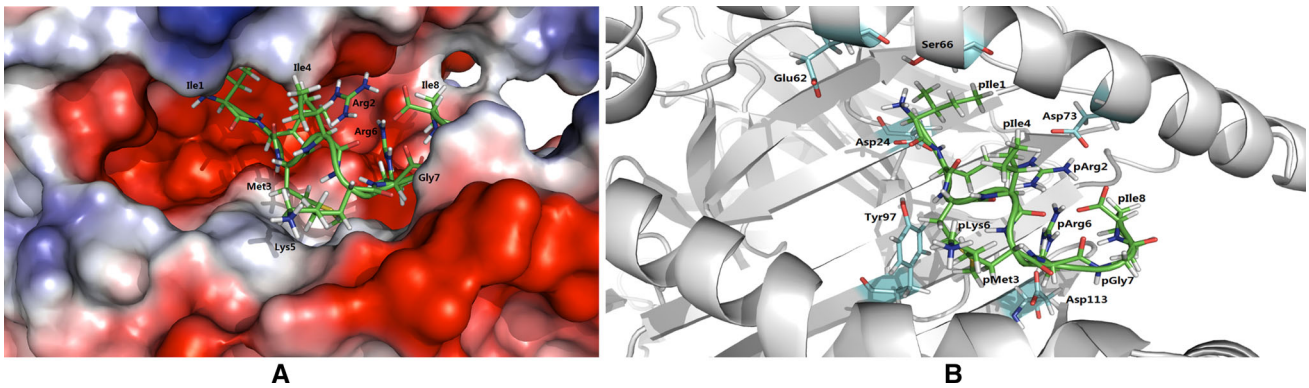

Fig. 9 The lowest potential energy conformation of BF2*15-IRMIKRGI octapeptide complex, shown as electrostatic potential surface (A) and sticks as well as cartoons (B)

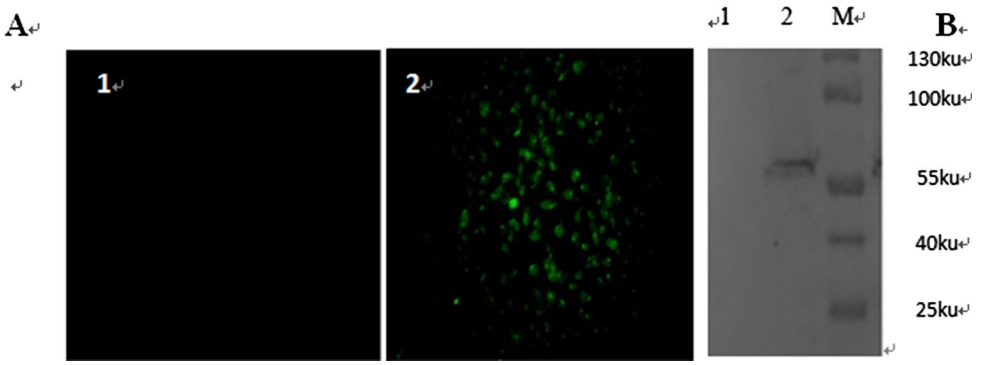

Fig. 10 Expression of pCAGGS-NP *in vitro.* **A**; IFA result of 293T cells transfected with pCAGGS-NP. 293T cells were transfected with pCAGGS-NP or empty pCAGGS plasmids. After 48 hours, IFA was performed using the polyclonal antiserum from a chicken infected with H5N1virus A/Goose/Guangdong/1/1996. A: 1. pCAGGS; B. pCAGGS-NP. (magnifications are × 400). **B**; Western blot analysis of the recombinant protein H5N1-NP expressed in 293T cells transfected with pCAGGS-NP. SDS-PAGE analysis showed that cells transfected with the pCAGGS-NP produced a large amount of protein with a molecular mass of approximately 62 ku, consistent with the expected molecular weight of the NP protein (data not shown). Furthermore, western blot analysis using polyclonal antiserum confirmed the expression of NP (lane 2), while there was no such signal at the corresponding position of the negative control sample (lane 1). Lane M, prestained protein mass marker; lane 1, pCAGGS vector; lane 2, recombinant pCAGGS-NP protein

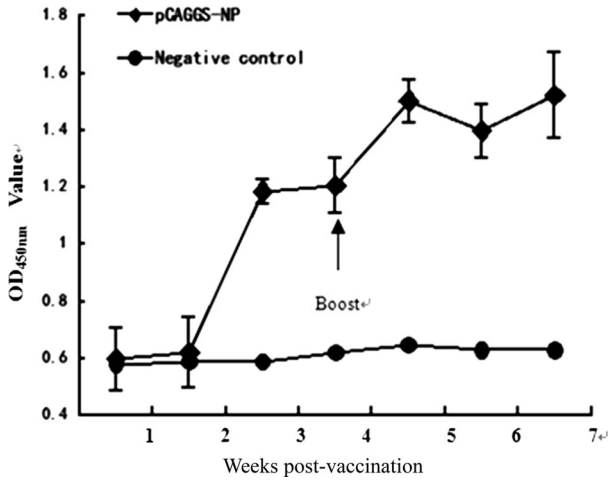

Fig. 11 NP antibody response in chickens vaccinated with plasmid pCAGGS-NP. A significant NP increase in the amount of antibody was detected at two weeks post-immunisation in chickens immunised with pCAGGS-NP compared with chickens in the control group ($P < 0.01$), which increased further after the boost and remained at a high level until the end of the experiment

Activation of lymphocytes using peptides

To verify the predicted T-cell epitopes in NP, five synthetic peptides (four predicted peptides from NP and one unrelated peptide $N_{71–78}$) were incubated with sensitized splenic lymphocytes for three days. The results of the flow cytometric analysis showed that the proliferation of CD8+T lymphocytes increased by 41.8 %, 2.6 %, 2.2 %, 2.3 %, 0.1 %, and 0 in the cells stimulated with peptides $NP_{67–74}$, $NP_{120–128}$, $NP_{163–170}$, $NP_{85–92}$, $NP_{71–78}$, and the control, respectively (Fig. 12). After polypeptide stimulation, the copy number of the IFN-γ mRNA was significantly higher in splenic lymphocytes stimulated by $NP_{67–74}$ than in the control group and the other four groups ($P \leq 0.05$) (Fig. 13). This result shows that $NP_{67–74}$ can stimulate avian lymphocytes to secrete IFN-γ, and this cellular toxicity elicits a response from the T lymphocytes. Thus, $NP_{67–74}$ is a potential T-cell epitope polypeptide.

Discussion

On the basis of the identification of the BF2*15 binding motif, this study predicted and experimentally identified the CTL epitopes from the NP of H5N1 (A/Goose/Gongdong/1/96) virus for the MHC class I (BF2*15) in chickens. Computational analysis, including homology modeling, MD simulation, and molecular docking, showed that Arg2 and Arg6 of the IBV octapeptide acted as anchor residues and interacted with Asp24/Asp73 and Asp73/Asp113 of BF2*15, respectively. Thus, we conclude that the P2 and P6 positions of the BF2*15 binding peptide are positively charged. We further screened four octapeptides containing the motif "x-Arg/Lys-x-x-x-Arg/Lys" from the H5N1 NP by molecular docking and MD simulation. One

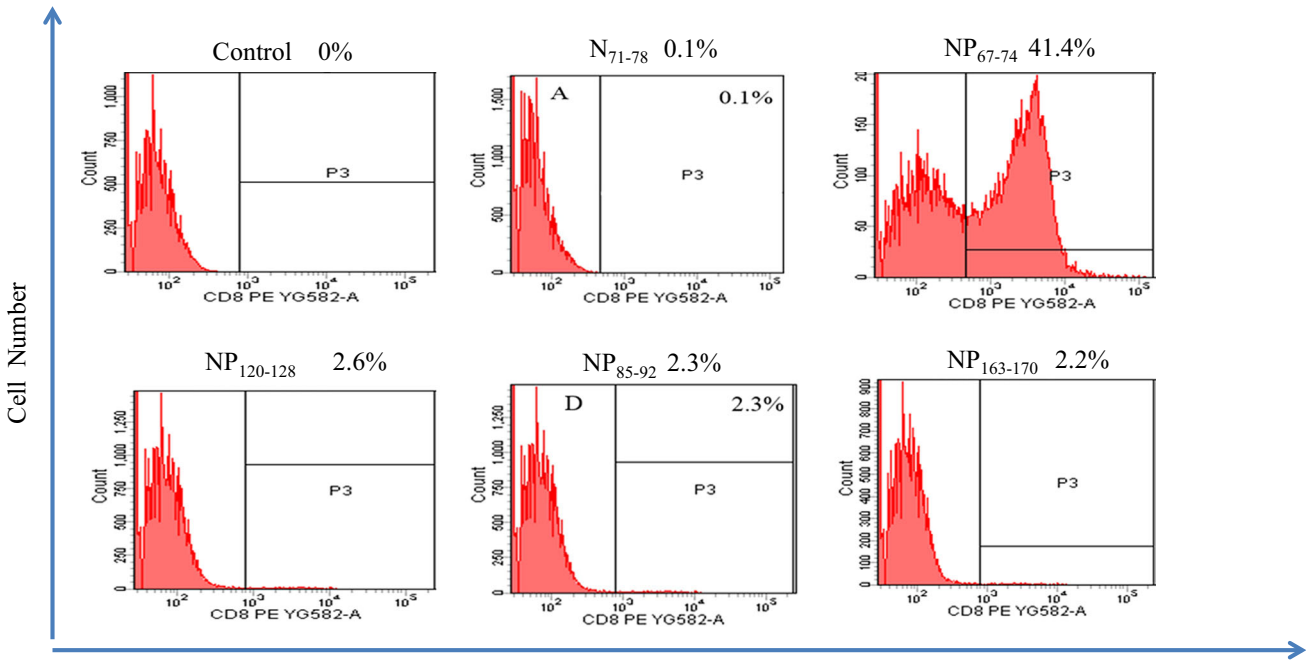

Fig. 12 CD8+ T cell proliferation after stimulation. The control was normal spleen lymphocytes. The NP67-74 group was spleen lymphocytes stimulated with NP67-74, whereas the NP67-74, NP120-128, NP85-92,NP163-170 and N71-78 groups were spleen lymphocytes stimulated with NP67-74, NP120-128, NP85-92,NP163-170 and irrelevant peptide N71-78. CD8+T cells were labeled using CESF and detected using a Cytomics FC 500 MCL flow cytometer (Beckman)

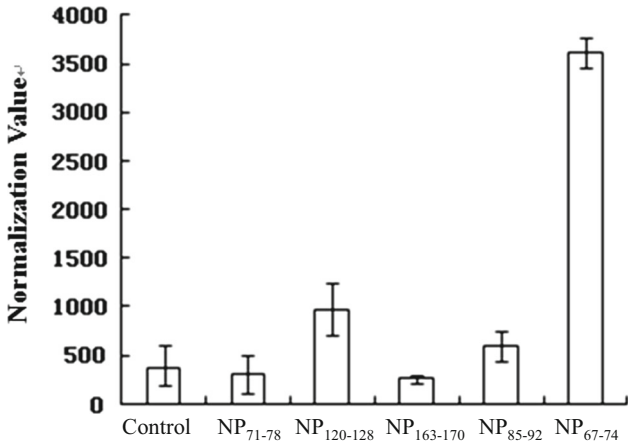

Fig. 13 IFN-γ mRNA expression from the immunized chicken splenic lymphocytes stimulated with peptides *in vitro*. After removing the test error and after normalising for copy number, the NP67-74-stimulated splenic lymphocytes show the highest IFN-γ normalisation value. Moreover, the normalised value was significantly higher for the IFN-γ gene than for the control group and the other four groups. ($p \leq 0.05$)

of the octapeptides passed experimental validation. Notably, the motifs differed from those of a previous study conducted by Wallny et al. [53, 54]. The motifs in this study were obtained from a complex structure; hence, the results may be more reliable. Concurrently, we also noted that B2 shared 24 and 73 identical residues with B15 (Table 1) and thus should possess similar P2 residues. However, the P2 residues of the B2 binding peptide are Pro (4CVX) and Ile (4D0D), respectively. Both Pro and Ile are hydrophobic, medium-sized residues with no charge and therefore differ greatly from Arg and Lys. These differences may be induced by the distinct residue at the ninth position, which lay between Asp24 and Asp73. In B15 and B2, the ninth residue was Ser and Arg, respectively. Ser9 possessed a small-sized side chain with no charge, hence allowing the interaction between Arg2 and Asp24/Asp73. Meanwhile, Arg9 was positively charged and possessed a bulged side chain. Thus, the residue would provide both repulsive force and steric hindrance to break the interaction between Arg2 and Asp24/Asp73. These theories may help explain the difference between B2 and B15 at position 2. For B14, the 73rd and 113th residues were the same as those of B15. Therefore, position P6 of B14 should also be positively charged. However, the P6 of B14 (4CW1) was Pro instead of Arg or Lys. This finding may be explained by the possibility that Lys9, instead Pro6, of the B14 binding peptide interacted with Asp73/Asp113, similar to the behavior of Arg6 of the B15 binding peptide.

Eight octapeptides were initially found in the H5N1 influenza virus NP protein by sequence analysis (Table 2). Considering that the BF2*15 groove was extremely negatively charged, the octapeptides with exceedingly numerous negatively charged residues, such as "DKEEIRRI" and "DRNFWRGE," were excluded first. Furthermore, docking analysis indicated that Arg at P3 position considerably facilitated octapeptide binding. Hence, "GKDPKKTG" was also excluded for its negatively charged Asp3. To further analyze the interaction between the peptides and BF2*15, the conformation in solvent of the remaining five peptides were explored using MD simulations. Specifically, each peptide was simulated with four trajectories for 50 ns, and the structure with the lowest potential energy was selected and used for molecular docking. Only the conformations with the highest ZDOCK scores, as well as those with anchor residues that interacted with Asp24, Asp73, and Asp113 were selected because the P2 and P6 residues were identified as the anchor residues in this study. On the basis of the MD simulation analysis, the peptide "TRVAPRGQ" was also excluded because the octapeptide dissociated from the BF2*15 groove rapidly. By contrast, "RRRDGKWV" (designated as $NP_{67–74}$) formed a stable conformation with BF2*15 (Fig. 7), which partly occupied the BF2*15 groove. However, the peptide's interaction mode differed from that of the IBV octapeptide (WRRQARYK) (Fig 6.). Specifically, the Arg1 side chain, instead of the main chain, interacted with BF2*15 Glu62 as well as Asp24. On the other hand, Arg2 interacted with Asp73/Asp113 and replaced the position of Lys6. Although the binding mode was dissimilar, we still retained this peptide because the interaction was stable during the entire simulation process, with multiple salt bridges and hydrogen bonds formed between the peptide and BF2*15.

Table 1 The initially predicted peptide sequence of NP from H5N1

Peptide number	Position	Peptide sequence
NP1	NP_{86-93}	GKDPKKTG
NP2	NP_{67-74}	RRRDGKWV
NP3	$NP_{112-119}$	DKEEIRRI
NP4	NP_{85-92}	IRRIWRQA
NP5	$NP_{120-128}$	TRALVRTG
NP6	$NP_{163-170}$	IRMIKRGI
NP7	$NP_{203-210}$	DRNFWRGE
NP8	$NP_{350-357}$	TRVAPRGQ

Table 2 The sequence comparison of B15, B2, B4, B14 and B21

	Amino acid position		
	24	73	113
B15	Asp	Asp	Asp
B2	Asp	Asp	Met
B4	Thr	Gln	Ser
B14	Thr	Asp	Asp
B21	Asp	Gln	Ala

The peptide "TRALVRTG" (named $NP_{120–128}$) also bound with BF2*15 in a similar way to that of the IBV octapeptide. The peptide fully occupied the groove with a more extended conformation than that of the latter octapeptide. Two anchor residues, Arg2 and Arg6, interacted with Asp24/Asp73 and Asp73/Asp113, respectively. The free amino moiety of Thr1 formed a salt bridge with Glu62 and a hydrogen bond with Tyr156. Arg2 formed another hydrogen bond with Tyr97. Finally, the free carboxyl moiety of Gly8 produced an electrostatic interaction with Lys143. The third peptide "IRMIKRGI" (denoted as $NP_{163–170}$) also bound with BF2*15 (Fig 9.). However, the binding ability was weak, mainly due to the peptide's cyclic conformation. Specifically, the free carboxyl moiety of Ile8 interacted with Arg2 and Arg6, leading to weaker electrostatic interactions of Arg2/Arg6 and Asp24/Asp73/Asp113. Furthermore, the free carboxyl moiety of Ile8 failed to interact with Lys83 or Lys143.

The detection of antibodies against NP indicates that DNA vaccination with pCAGGS-NP likely drives the differentiation of memory B cells, which are subsequently activated following the booster immunization. Such a phenomenon may have resulted in increased NP-specific antibody titers, which is consistent with the result from the previous study [43]. On the basis of previous studies [42, 43], IFN-γ mRNA generated by spleen cells following peptide stimulus was evaluated using real-time RT-PCR. IFN-γ production of cell supernatants was detected using capture ELISA. The results showed that the peptide $NP_{67–74}$ not only induced the highest level of IFN-γ mRNA but also stimulated IFN-γ production relative to that in the control ($P < 0.01$). The subsequent $CD8^+$ T-lymphocyte proliferation assay confirmed this result. By combining these results with those of computational analysis, the NP67-74 peptides were identified bioinformatically as the CTL epitope in chickens of the BF2*15 haplotype.

The mapping of CTL epitopes is very important in the design of synthetic vaccines and understanding the immune mechanisms involved in the clearance of viral infection. To the best of our knowledge, understanding is limited on the specific H5N1-derived peptides targeted by T cells in chickens. To date, only two reports have discussed T-cell epitopes from the NP and HA of the H5N1 virus in chickens [42, 43]. However, these peptides have not been identified to specific haplotypes, except for the $H5_{246–260}$ from the HA1 domain, which was identified as the dual-specific epitope for both major MHC class I and II molecules of the B^{19} haplotype in chicken [42]. In this study, through computational analysis of the interaction between the IBV octapeptide and BF2*15, we explored the binding motif of BF2*15, predicted the CTL epitopes from the NP of H5N1 (A/Goose/Gongdong/1/96) virus for MHC class I (BF2*15) in chickens based on the explored motif. We then eventually identified the $NP_{67–74}$ peptide as the CTL epitope of the BF2*15 haplotype in chickens using experimental methods. These results will help to increase our understanding of the immune mechanism of the H5N1 virus in chickens. Influenza viruses are known to evade host immunity frequently via antigenic drift and shift despite previous influenza virus infection and/or vaccination [55]. Therefore, vaccines that match circulating viral strains are needed for optimal protection [56]. This notion implies that the development of a universal influenza virus vaccine providing broadly cross-protective immunity is of great importance. The NP of influenza A virus is highly conserved among all strains of influenza A viruses and has been explored as an antigen for the development of a universal influenza virus vaccine [56]. The most recent study on this topic showed that the incorporation of a conserved NP of the H5N1 virus into influenza virus-like particles (VLPs) could provoke more-robust humoral and cellular immune responses in chickens when compared with the VLPs without NP [57]. This finding means that the immune responses against the conserved NP might play an important defensive role against influenza virus. The peptide $NP_{67–74}$, which was identified in this study as the CTL epitope in BF2*15 of chickens, may help interpret these immune mechanisms.

By using homology modeling, MD simulation, and molecular docking approaches, this study explored the motif of BF2*15 MHC class I and further identified the peptide $NP_{67–74}$ as the CTL epitope in chicken BF2*15. The study methods can also aid in predicting CTL epitopes for other pathogens of chickens. Furthermore, the results of this study also help in achieving a deeper understanding of the immune mechanisms of avian influenza virus.

Acknowledgments This study was supported by the Modern Agro-Industry Technology Research System (CARS-42), Chinese Special Fund for Agro-Scientific Research in the Public Interest (201303033), and National Key Research and Development Plan (2016YFD0500200). No competing interests exist.

Reference

1. Webster RG, Bean WJ, Gorman OT, Chambers TM, Kawaoka Y (1992) Evolution and ecology of influenza A viruses. Microbiol Rev 56:152–179
2. Du L, Jin L, Zhao G, Sun S, Li J, Yu H et al (2013) Identification and structural characterization of a broadly neutralizing antibody targeting a novel conserved epitope on the influenza virus H5N1 hemagglutinin. J Virol 87:2215–2225
3. Webster RG (2002) The importance of animal influenza for human disease. Vaccine 20(Suppl 2):S16–S20
4. Claas EC, Osterhaus AD, van Beek R, De Jong JC, Rimmelzwaan GF, Senne DA et al (1998) Human influenza A H5N1 virus related to a highly pathogenic avian influenza virus. Lancet 351:472–477

5. Yuen KY, Chan PK, Peiris M, Tsang DN, Que TL, Shortridge KF et al (1998) Clinical features and rapid viral diagnosis of human disease associated with avian influenza A H5N1 virus. Lancet. 351:467–471
6. Subbarao K, Klimov A, Katz J, Regnery H, Lim W, Hall H et al (1998) Characterization of an avian influenza A (H5N1) virus isolated from a child with a fatal respiratory illness. Science 279:393–396
7. Parida R, Shaila MS, Mukherjee S, Chandra NR, Nayak R (2007) Computational analysis of proteome of H5N1 avian influenza virus to define T cell epitopes with vaccine potential. Vaccine 25:7530–7539
8. Thomas PG, Keating R, Hulse-Post DJ, Doherty PC (2006) Cell-mediated protection in influenza infection. Emerg Infect Dis 12:48–54
9. Boni MF, Gog JR, Andreasen V, Feldman MW (2006) Epidemic dynamics and antigenic evolution in a single season of influenza A. Proc Biol Sci 273:1307–1316
10. Watanabe Y, Arai Y, Daidoji T, Kawashita N, Ibrahim MS, El-Gendy Eel D et al (2015) Characterization of H5N1 influenza virus variants with hemagglutinin mutations isolated from patients. MBio. 6:00081–00095
11. Cohen J (2012) Bird flu controversy. Does forewarned = fore-armed with lab-made avian influenza strains? Science 335:785–787
12. Harada Y, Ninomiya-Mori A, Takahashi Y, Shirakura M, Kishida N, Kageyama T et al (2011) Inactivated and adjuvanted whole-virion clade 2.3.4 H5N1 pre-pandemic influenza vaccine possesses broad protective efficacy against infection by heterologous clades of highly pathogenic H5N1 avian influenza virus in mice. Vaccine. 29:8330–8337
13. Huang MH, Lin SC, Hsiao CH, Chao HJ, Yang HR, Liao CC et al (2010) Emulsified nanoparticles containing inactivated influenza virus and CpG oligodeoxynucleotides critically influences the host immune responses in mice. PLoS One 5:e12279
14. Steel J (2011) New strategies for the development of H5N1 subtype influenza vaccines: progress and challenges. BioDrugs 25:285–298
15. Ding H, Tsai C, Gutierrez RA, Zhou F, Buchy P, Deubel V et al (2011) Superior neutralizing antibody response and protection in mice vaccinated with heterologous DNA prime and virus like particle boost against HPAI H5N1 virus. PLoS One 6:e16563
16. Hessel A, Schwendinger M, Holzer GW, Orlinger KK, Coulibaly S, Savidis-Dacho H et al (2011) Vectors based on modified vaccinia Ankara expressing influenza H5N1 hemagglutinin induce substantial cross-clade protective immunity. PLoS One 6:e16247
17. Khurana S, Wu J, Verma N, Verma S, Raghunandan R, Manischewitz J et al (2011) H5N1 virus-like particle vaccine elicits cross-reactive neutralizing antibodies that preferentially bind to the oligomeric form of influenza virus hemagglutinin in humans. J Virol 85:10945–10954
18. Ledgerwood JE, Wei CJ, Hu Z, Gordon IJ, Enama ME, Hendel CS et al (2011) DNA priming and influenza vaccine immunogenicity: two phase 1 open label randomised clinical trials. Lancet Infect Dis 11:916–924
19. Lin SC, Huang MH, Tsou PC, Huang LM, Chong P, Wu SC (2011) Recombinant trimeric HA protein immunogenicity of H5N1 avian influenza viruses and their combined use with inactivated or adenovirus vaccines. PLoS One 6:e20052
20. Suguitan AL Jr, Cheng X, Wang W, Wang S, Jin H et al (2011) Influenza H5 hemagglutinin DNA primes the antibody response elicited by the live attenuated influenza A/Vietnam/1203/2004 vaccine in ferrets. PLoS One 6:e21942
21. Torrieri-Dramard L, Lambrecht B, Ferreira HL, Van den Berg T, Klatzmann D, Bellier B (2011) Intranasal DNA vaccination induces potent mucosal and systemic immune responses and cross-protective immunity against influenza viruses. Mol Ther 19:602–611
22. Charles A, Janeway J, Paul T, Mark W, Mark J (2001) Immunobiology: the immune system in health and disease, 5th edn. Garland Science, New York
23. Sette A, Peters B (2007) Immune epitope mapping in the post-genomic era: lessons for vaccine development. Curr Opin Immunol 19:106–110
24. Sette A, Fleri W, Peters B, Sathiamurthy M, Bui HH, Wilson S (2005) A roadmap for the immunomics of category A-C pathogens. Immunity 22:155–161
25. Bui HH, Sidney J, Dinh K, Southwood S, Newman MJ, Sette A (2006) Predicting population coverage of T-cell epitope-based diagnostics and vaccines. BMC Bioinform 7:153
26. Goodman AG, Heinen PP, Guerra S, Vijayan A, Sorzano CO, Gomez CE et al (2011) A human multi-epitope recombinant vaccinia virus as a universal T cell vaccine candidate against influenza virus. PLoS One 6:e25938
27. Gogolak P, Simon A, Horvath A, Rethi B, Simon I, Berkics K et al (2000) Mapping of a protective helper T cell epitope of human influenza A virus hemagglutinin. Biochem Biophys Res Commun 270:190–198
28. Cheong WS, Reiseger J, Turner SJ, Boyd R, Netter HJ (2009) Chimeric virus-like particles for the delivery of an inserted conserved influenza A-specific CTL epitope. Antiviral Res 81:113–122
29. Terajima M, Jameson J, Norman JE, Cruz J, Ennis FA (1999) High-yield reassortant influenza vaccine production virus has a mutation at an HLA-A 2.1-restricted $CD8^+$ CTL epitope on the NS1 protein. Virology 259:135–140
30. Ostankovitch M, Guichard G, Connan F, Muller S, Chaboissier A, Hoebeke J et al (1998) A partially modified retro-inverso pseudopeptide modulates the cytokine profile of CTL specific for an influenza virus epitope. J Immunol 161:200–208
31. Babin C, Majeau N, Leclerc D (2013) Engineering of papaya mosaic virus (PapMV) nanoparticles with a CTL epitope derived from influenza NP. J Nanobiotechnol 11:10
32. Zhong W, Dixit SB, Mallis RJ, Arthanari H, Lugovskoy AA, Beveridge DL et al (2007) CTL recognition of a protective immunodominant influenza A virus nucleoprotein epitope utilizes a highly restricted Vbeta but diverse Valpha repertoire: functional and structural implications. J Mol Biol 372:535–548
33. Rammensee H, Bachmann J, Emmerich NP, Bachor OA, Stevanovic S (1999) SYFPEITHI database for MHC ligands and peptide motifs. Immunogenetics 50:213–219
34. Parker KC, Bednarek MA, Coligan JE (1994) Scheme for ranking potential HLA-A2 binding peptides based on independent binding of individual peptide side-chains. J Immunol 152:163–175
35. Zhang GL, Srinivasan KN, Veeramani A, August JT, Brusic V (2005) PREDBALB/c: a system for the prediction of peptide binding to H2d molecules, a haplotype of the BALB/c mouse. Nucleic Acids Res 33:W180–W183
36. Nielsen M, Lundegaard C, Worning P, Hvid CS, Lamberth K, Buus S et al (2004) Improved prediction of MHC class I and class II epitopes using a novel Gibbs sampling approach. Bioinformatics 20:1388–1397
37. Bui HH, Sidney J, Peters B, Sathiamurthy M, Sinichi A, Purton KA et al (2005) Automated generation and evaluation of specific MHC binding predictive tools: ARB matrix applications. Immunogenetics 57:304–314
38. Peters B, Sette A (2005) Generating quantitative models describing the sequence specificity of biological processes with the stabilized matrix method. BMC Bioinform 6:132
39. Larsen MV, Lundegaard C, Lamberth K, Buus S, Brunak S, Lund O et al (2005) An integrative approach to CTL epitope prediction:

a combined algorithm integrating MHC class I binding, TAP transport efficiency, and proteasomal cleavage predictions. Eur J Immunol 35:2295–2303
40. Nielsen M, Lundegaard C, Worning P, Lauemoller SL, Lamberth K, Buus S et al (2003) Reliable prediction of T-cell epitopes using neural networks with novel sequence representations. Protein Sci 12:1007–1017
41. Moutaftsi M, Peters B, Pasquetto V, Tscharke DC, Sidney J, Bui HH et al (2006) A consensus epitope prediction approach identifies the breadth of murine T($CD8^+$)-cell responses to vaccinia virus. Nat Biotechnol 24:817–819
42. Haghighi HR, Read LR, Haeryfar SM, Behboudi S, Sharif S (2009) Identification of a dual-specific T cell epitope of the hemagglutinin antigen of an h5 avian influenza virus in chickens. PLoS One 4:e7772
43. Hou Y, Guo Y, Wu C, Shen N, Jiang Y, Wang J (2012) Prediction and identification of T cell epitopes in the H5N1 influenza virus nucleoprotein in chicken. PLoS One. 7:e39344
44. Liu G, Wang Q, Tong T, Xiao Y, Bai Y, Liu S et al (2008) Construction and functional test of a chicken MHC-I (BF2*15)/peptide tetramer. Vet Immunol Immunopathol 122:1–7
45. Boots AM, Kusters JG, van Noort JM, Zwaagstra KA, Rijke E, van der Zeijst BA et al (1991) Localization of a T-cell epitope within the nucleocapsid protein of avian coronavirus. Immunology 74:8–13
46. Brooks BR, Brooks CL 3rd, Mackerell AD Jr, Nilsson L et al (2009) CHARMM: the biomolecular simulation program. J Comput Chem 30:1545–1614
47. Theoroetical and Computational Biophysics Group. http://www.ks.uiuc.edu/. Accessed 22 Nov 2013
48. Vreven T, Pierce BG, Hwang H, Weng Z (2013) Performance of ZDOCK in CAPRI rounds 20-26. Proteins. 81:2175–2182
49. Lenstra JA, Kusters JG, Koch G, van der Zeijst BA (1989) Antigenicity of the peplomer protein of infectious bronchitis virus. Mol Immunol 26:7–15
50. Chappell P, el Meziane K, Harrison M, Magiera L, Hermann C, Mears L et al (2015) Expression levels of MHC class I molecules are inversely correlated with promiscuity of peptide binding. Elife 4:e05345
51. Zhang J, Chen Y, Qi J, Gao F, Liu Y, Liu J et al (2012) Narrow groove and restricted anchors of MHC class I molecule BF2*0401 plus peptide transporter restriction can explain disease susceptibility of B4 chickens. J Immunol 189:4478–4487
52. Koch M, Camp S, Collen T, Avila D, Salomonsen J, Wallny HJ et al (2007) Structures of an MHC class I molecule from B21 chickens illustrate promiscuous peptide binding. Immunity 27:885–899
53. Kaufman J, Volk H, Wallny HJ (1995) A "minimal essential Mhc" and an "unrecognized Mhc": two extremes in selection for polymorphism. Immunol Rev 143:63–88
54. Wallny HJ, Avila D, Hunt LG, Powell TJ, Riegert P, Salomonsen J et al (2006) Peptide motifs of the single dominantly expressed class I molecule explain the striking MHC-determined response to Rous sarcoma virus in chickens. Proc Natl Acad Sci USA 103:1434–1439
55. Li Y, Shi J, Zhong G, Deng G, Tian G, Ge J et al (2010) Continued evolution of H5N1 influenza viruses in wild birds, domestic poultry, and humans in China from 2004 to 2009. J Virol 84:8389–8397
56. Li Z, Gabbard JD, Mooney A, Gao X, Chen Z, Place RJ et al (2013) Single-dose vaccination of a recombinant parainfluenza virus 5 expressing NP from H5N1 virus provides broad immunity against influenza A viruses. J Virol 87:5985–5993
57. Xue C, Tian G, Chen X, Liu Q, Ma J, Xu S et al (2015) Incorporation of conserved nucleoprotein into influenza virus-like particles could provoke a broad protective immune response in BALB/c mice and chickens. Virus Res 195:35–42